

Modeling Deep Learning Accelerator Enabled GPUs

Md Aamir Raihan¹, Negar Goli^{* 1}, and Tor Aamodt¹

¹Electrical and Computer Engineering, University of British Columbia
{araihan, negargoli93, aamodt}@ece.ubc.ca

Abstract—The efficacy of deep learning has resulted in it becoming one of the most important applications run in data centers today. The NVIDIA Tesla V100 GPU introduced a specialized functional unit called the Tensor Core to meet growing demand for higher performance on this workload. To exploit the full capability of current NVIDIA GPUs machine learning researchers have started to use Tensor Cores. For example 5 out of 6, 2018 Gordon Bell Award Finalists used Tensor Cores in their work. However, currently no open-source GPU micro-architectural simulators model Tensor Cores. In this paper, we comprehensively investigate NVIDIA’s Tensor Core implementation found in Volta and Turing architectures and propose an architectural model for it. Our Tensor Core timing model, implemented in GPGPU-Sim, achieves 99.6% IPC correlation versus a physical V100 GPU. Building upon this we also enable GPGPU-Sim to run NVIDIA’s CUTLASS, an open-source CUDA C++ templates library providing customizable GEMM templates including the support for Tensor Cores.

Index Terms—Tensor Core, Tesla V100, CUTLASS library

I. INTRODUCTION

Deep learning based data analytics has recently emerged as an important technique. Deep Neural Networks (DNNs) have enabled breakthroughs in speech recognition [1], [2], image recognition [3], [4] and computer vision [5], [6]. These benefits come at the expense of high computational cost. DNNs perform dense matrix (tensor) computations and recent research has explored how to accelerate these operations [7]–[14] and many companies are developing custom hardware for these workloads. GPUs are commonly used for deep learning, especially during training, as they provide order of magnitude higher performance versus a comparable investment in CPUs.

Recently, NVIDIA released GPUs containing a specialized computing unit called the Tensor Core to accelerate tensor operations. The NVIDIA Tesla V100 GPU equipped with Tensor Cores provide a theoretical peak performance of up to 125 TFLOPS. However, few details of the underlying design of Tensor Cores have been disclosed by NVIDIA. In this paper, we investigate the design of NVIDIA Tensor Cores. Based upon our analysis we add functional and timing models for NVIDIA Tensor Cores to GPGPU-Sim. We also make changes to enable the NVIDIA CUTLASS library, an open source template library providing efficient customizable GEMM template including support of tensor cores, run on GPGPU-Sim. This provides a framework to investigate micro-architectural changes to deep learning enabled GPUs.

* equal contribution

A. Volta Microarchitecture

Volta is the first NVIDIA GPU architecture which is powered by Tensor Cores. Its architecture is significantly different from its predecessor Pascal [15]. Its Shader Module (SM) is redesigned for performance and energy efficiency. Each Volta SM has twice the scheduling logic compared to Pascal, separate integer and 32-bit floating point (FP32) cores and additional Tensor Cores. As shown in Figure 1 Volta SM has a L1 instruction cache, 128 KB combined L1 data cache and shared memory (SMEM), a texture (TEX) unit, and four Sub-Cores.

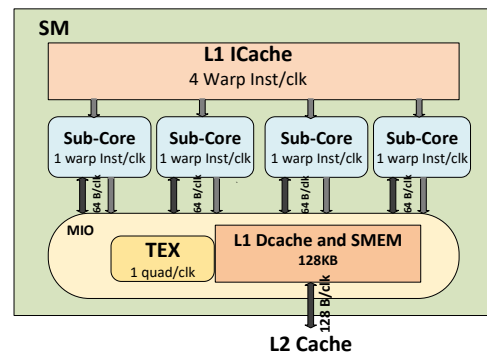


Fig. 1: Volta SM(reproduced from Slides [16])

Volta's SM is partitioned into four processing blocks (Sub-Cores), each with 1 warp scheduler and 1 dispatch unit per scheduler whereas Pascal's SM is partitioned into two blocks, each with 1 warp scheduler and 2 dispatch units per scheduler. The absence of a second dispatch unit associated with the scheduler implies that each warp scheduler can dispatch only one instruction per clock and is not able to dispatch a second independent instruction. Thus, the warp scheduler in no way can exploit the Instruction level parallelism(ILP). Though Volta's SM has twice warp scheduler compared to Pascal SM which keeps the same throughput. Each Volta Sub-Core has 16 FP16 cores, 16 INT32 cores, 8 FP64 cores, 2 Tensor Cores, L0 instruction cache, 1 Warp scheduler, 1 Dispatch unit, and 64 KB register files as shown in Figure SubCoreMicroarchitecture. The warp scheduler directly issues tensor operations to Tensor Core and branch instructions to branch unit whereas for all the other cores it is dispatched from the math dispatch unit. Once the tensor operation is issued to the tensor cores it waits for the input matrices from the register file and performs the 4x4 matrix multiply

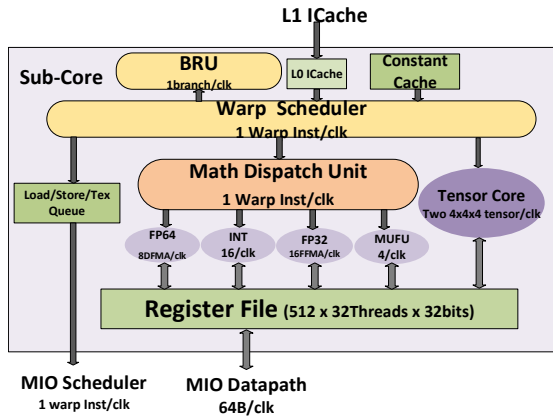


Fig. 2: Sub-Core inside SM(reproduced from Slides [16])

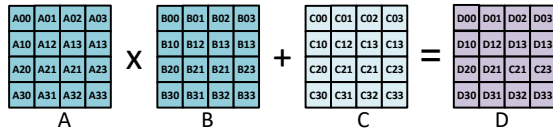


Fig. 3: Tensor core 4×4 MACC ($D = A * B + C$) per cycle

and accumulate operation and stores the final results back to the register file. While a V100 SM has the same number of registers as compared to Pascal SM, the entire V100 GPU has far more SMs and thus has many more registers which can support more threads, warps, and thread blocks compared to prior generations GPUs.

B. Tensor Core

Tensor Core is a specialized programmable compute unit for accelerating machine learning workload. The Tesla V100 GPU contains 640 Tensor Cores distributed across 80 SMs, with 8 Tensor Cores per SM, providing a theoretical performance of 125 tensor TFLOPS at an operational frequency of 1530MHZ. Each Tensor Core performs 4×4 matrix-multiply-and-accumulation (MACC) in one clock cycle i.e. $D = A \times B + C$ where A, B, C are 4×4 matrices as shown in Figure 3. The Tensor Core can operate in two modes: FP16 and mixed precision mode. In FP16 mode the Tensor Core takes three FP16 matrices whereas in the mixed precision mode it takes two FP16 matrices with the third accumulation matrix being either FP16 or FP32. NVIDIA provides four programming interfaces for using Tensor Cores: the CUDA Warp Matrix Multiply Accumulate(WMMA) API and three CUDA libraries: cuBLAS [17], cuDNN [18] [19] and CUTLASS [20] [21]. Furthermore, many deep learning frameworks have included support for Tensor Cores.

C. WMMA API

It is the only interface provided by NVIDIA for directly programming the Tensor Core. It exposes Tensor Cores as a warp level operation and always operates on fixed tile size for performing the matrix MACC operation. The tile size is represented by the tuple $M \times N \times K$ where $M \times K$ is the dimension

of Matrix A and $K \times N$ is the dimension of Matrix B. Cuda 9.0 only supports $16 \times 16 \times 16$ tile size. The input matrices are distributed across different threads, each thread contains only a fragment of the entire matrix. WMMA API provides three new functions, `load_matrix_sync`, `store_matrix_sync` and `mma_sync`. `load_matrix_sync` and `store_matrix_sync` are used for loading and storing the input matrices to the fragments and `mma_sync` performs warp synchronous matrix multiply and accumulate operation. All the three functions wait for thread convergence before performing the load, store or matrix MACC operation.

D. PTX Instruction Set

NVIDIA introduces three PTX (parallel thread execution) instructions, a pseudo-assembly language used in NVIDIA's CUDA programming environment, exclusively for tensor core:

- `wmma.load.a.sync.layout.shape.type r, [p], stride;`
- `wmma.mma.sync.alayout.blayout.shape.dtype.ctype d, a, b, c;`
- `wmma.store.d.sync.layout.shape.type r, [p], stride;`

where sync qualifier indicates that all the above instructions wait for synchronization before beginning execution, layout qualifier specifies whether the operand matrices is stored in row-major or column-major. Qualifier type represents the precision of the operand matrices i.e. FP16 or FP32, here, A and B matrices should be FP16 but C matrix can be either FP16 or FP32. Shape qualifier represents the shape of the operand matrices. Loading the matrices A, B and C from the memory to the register-file are performed using the `wmma.load` PTX instruction. `wmma.load.a`, `wmma.load.b` and `wmma.load.c` load the A,B and C matrices respectively. `wmma.load` will load the entire 16×16 matrix inside the warp, thus each thread only needs to load 8 elements but in `wmma.load` each thread loads 16 elements from the operand matrix i.e. every element of the input matrix is loaded twice. `wmma.load` supports strided load since the 16×16 matrix loaded from the memory can be a sub-part of a larger matrix, thus stride specifies the beginning of each row(or column) to the next depending upon the layout of the matrix in the memory.

`wmma.mma` performs warp level matrix multiply and accumulate operation i.e. computes $D = A \times B + C$ using registers a, b and c which contains the matrix A, B and C respectively. The computed results are stored in registers d in each thread. Similarly `wmma.store` stores the computed matrix from the registers d to the memory. It also supports strided store.

II. REVERSE ENGINEERING TENSOR CORES

In the previous section, we discussed the high-level details which were provided by NVIDIA about the Tensor Core. In this section, we will provide the intricate details found during the extensive profiling and analysis of SASS code. To simplify the discussion below, we define some of the common terminologies which will be used throughout the rest of the paper. Group of four consecutive threads forms a *threadgroup*.

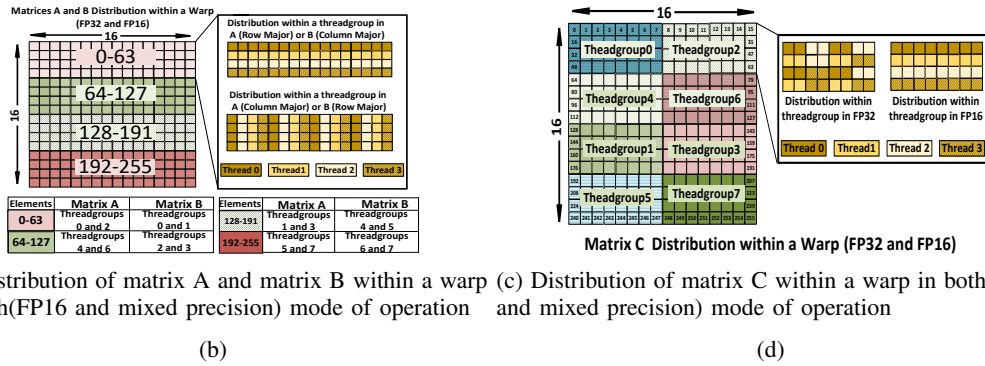


Fig. 4: Distribution of matrix fragments A,B and C in different layout in V100 GPU

There are 8 *threadgroups* in a warp and the *threadgroup* id of any thread is $\lfloor \frac{threadIdx}{4} \rfloor$.

A. Matrix Distribution Over Fragment in Volta Tensor Cores

Nvidia doesn't disclose the distribution of the matrix fragments loaded by different threads. Jia et al [22] was the first one who found the distribution of matrix fragments but they only showed the distribution for mixed precision mode in column-major layout. We find the distribution for both mode of operation and all the different layout combination for matrices A, B, and C as shown in Figure 4. In Figure 4 cell value represents the relative position of the element in 1-D layout i.e. index 4 represent the fourth element in the 1-D layout.

Each element of the matrix are loaded by two threads in a warp and thus the entire matrix is loaded twice. For matrix A and B in both modes of operation, each *threadgroup* load 16×4 segments of the matrix and each of these segments is loaded by two different *threadgroups*. As shown in Figure 4b the first four consecutive row is loaded by *threadgroup* 0 and 2. The distribution of matrix A stored in row-major layout is same as the distribution of matrix B stored in a column-major layout and vice-versa. For the matrix A in row-major layout, each thread inside the *threadgroup* loads 16 consecutive elements as shown in Figure 4b whereas in column major layout each thread inside the *threadgroup* loads four blocks of four consecutive elements with a stride distance of 64 elements as shown in Figure 4b. For matrix C, the distribution of matrix is different from the distribution of A and B. Here, each *threadgroup* loads either 8×4 segment of the matrix C and the distribution within the threadgroup depends on whether the matrix C is stored in FP16 or FP32 format as shown in Figure 4d and 4d.

B. Disassembled SASS assembly in Volta Tensor Cores

SASS code is an intermediate ISA, sometimes called shader assembly, exists in between PTX and binary code, targeting a specific device. It is the actual ISA interface for programming the GPU. Nvidia introduces only one new SASS instruction, HMMA, for programming Tensor Core. It corresponds to the *wmma.mma* PTX instruction. Each HMMA instruction has four operands and each operand uses a pair of registers (in

HMMA instructions each pair of registers is shown by just the name of one of the register i.e the $\langle R8, R7 \rangle$ register pair is shown just by putting R8 in the HMMA instruction). The first operand register pair ($\langle R8, R7 \rangle$ as shown in the first line of Figure 5) is the destination register followed by three source operands ($\langle R24, R23 \rangle$, $\langle R22, R21 \rangle$ and $\langle R8, R7 \rangle$) each corresponding to operand matrices A, B, and C respectively. The input operand reuse flag is set for an operand if the operand is going to be reused in the next step. The operand is cached in the operand reuse cache and thus avoiding register fetch and possibly reducing bank conflict.

Every *wmma.mma* PTX instruction is broken into a group of HMMA instructions. In the FP32 mode in which matrix C is an FP32 matrix, each *wmma.mma* is broken into 16 HMMA instructions consisting of four sets. Each set comprises four steps as shown in Figure 5 whereas in FP16 mode, *wmma.mma* is broken into four sets like the FP32 mode but each set consists of only 2 steps. The table in the Figure 5 shows the cumulative clock cycles needed to complete the execution until the n^{th} HMMA. The cumulative clock cycles needed for executing *wmma.mma* API in mixed precision mode is 10 cycles less than that needed in the FP16 mode which demonstrates the interesting fact of faster *wmma.mma* execution in mixed precision mode rather than the FP16 mode.

NVIDIA doesn't provide any official documentation for the SASS instructions and thus there is no information about it. The first work for decoding the sets and steps in the disassembled SASS was done by Zhe Jia et al., [22] but they didn't demonstrated the experimental procedure in their report. Moreover, they only work on mixed precision mode. We not only recreate the results through our experiments but also observe that sets and steps behave differently in the FP16 mode as compared to mixed precision mode.

In order to find the role of the sets and the steps, we create a custom matrix multiply kernel using the WMMA API on the smallest input size. Our kernel only have one *wmma.mma* PTX instruction and the binary of this kernel consist of 16 HMMA instructions. We reverse engineered the binary to replace the occurrence of 15 HMMA instruction with NOP except a single HMMA instruction whose execution we want to determine. We patched the binary with the help of radare2 which is a

MIXED PRECISION MODE		Cumulative Clock Cycles
SET 1	HMMA.884.F32.F32.STEP0 R8, R24.reuse.COL, R22.reuse.ROW, R8;	10
	HMMA.884.F32.F32.STEP1 R10, R24.reuse.COL, R22.reuse.ROW, R10;	12
	HMMA.884.F32.F32.STEP2 R4, R24.reuse.COL, R22.reuse.ROW, R4;	14
	HMMA.884.F32.F32.STEP3 R6, R24.COL, R22.ROW, R6;	18
SET 2	HMMA.884.F32.F32.STEP0 R8, R20.reuse.COL, R18.reuse.ROW, R8;	20
	HMMA.884.F32.F32.STEP1 R10, R20.reuse.COL, R18.reuse.ROW, R10;	22
	HMMA.884.F32.F32.STEP2 R4, R20.reuse.COL, R18.reuse.ROW, R4;	24
	HMMA.884.F32.F32.STEP3 R6, R20.COL, R18.ROW, R6;	28
SET 3	HMMA.884.F32.F32.STEP0 R8, R14.reuse.COL, R12.reuse.ROW, R8;	30
	HMMA.884.F32.F32.STEP1 R10, R14.reuse.COL, R12.reuse.ROW, R10;	32
	HMMA.884.F32.F32.STEP2 R4, R14.reuse.COL, R12.reuse.ROW, R4;	34
	HMMA.884.F32.F32.STEP3 R6, R14.COL, R12.ROW, R6;	38
SET 4	HMMA.884.F32.F32.STEP0 R8, R16.reuse.COL, R2.reuse.ROW, R8;	40
	HMMA.884.F32.F32.STEP1 R10, R16.reuse.COL, R2.reuse.ROW, R10;	42
	HMMA.884.F32.F32.STEP2 R4, R16.reuse.COL, R2.reuse.ROW, R4;	44
	HMMA.884.F32.F32.STEP3 R6, R16.COL, R2.ROW, R6;	54

FP16 MODE		Cumulative Clock Cycles
SET 1	HMMA.884.F16.F16.STEP0 R4, R22.reuse.T, R12.reuse.T, R4;	12
	HMMA.884.F16.F16.STEP1 R6, R22.T, R12.T, R6;	21
SET 2	HMMA.884.F16.F16.STEP0 R4, R16.reuse.T, R14.reuse.T, R4;	25
	HMMA.884.F16.F16.STEP1 R6, R16.T, R14.T, R6;	34
SET 3	HMMA.884.F16.F16.STEP0 R4, R18.reuse.T, R8.reuse.T, R4;	38
	HMMA.884.F16.F16.STEP1 R6, R18.T, R8.T, R6;	47
SET 4	HMMA.884.F16.F16.STEP0 R4, R2.reuse.T, R10.reuse.T, R4;	51
	HMMA.884.F16.F16.STEP1 R6, R2.T, R10.T, R6;	64

Fig. 5: Disassembled SASS instructions corresponding to WMMA:MMA API

complete framework for reverse engineering and analyzing binary. Similarly, for finding the cumulative clock cycles for n^{th} HMMA as shown in Figure 5 we use our kernel and patched the binary to read the clock register before and after the 1^{st} and the n^{th} HMMA instruction.

Using the patched binary we found that in both the mode of operation i.e FP16 and mixed precision mode, during each set of HMMA instruction every *threadgroup* takes 4×4 segment of matrix A multiply it with a 4×8 segment of matrix B to produce a partial result which gets accumulated with a 4×8 segment of the accumulation tile. The accumulator tile is loaded with the matrix C thus during different steps within the set the partial product gets accumulated with the matrix C. During the four set, four rows of matrix A is multiplied with eight columns of matrix B to produce the final result for 4×8 segment of accumulation tile. Figure 6(a) shows the different segment of matrix A and matrix B taken in four sets for *threadgroup* 0.

In mixed precision mode each set is broken down into four steps and in each step 2×4 segment of matrix A is multiplied with 4×4 segment of matrix B and accumulated with 2×4 segment of matrix C. The segment of matrix A and matrix B taken in different steps within *threadgroup* 0 are shown in Figure 6(b) and Figure 6(e) shows the segments of the result matrix created by all the *threadgroups*.

In FP16 mode as shown in Figure 6(c), during each step of HMMA instructions each *threadgroup* takes 4×4 segment

of matrix A multiply it with 4×4 segment of matrix B and accumulate it with the accumulator tile. Figure 6(e) shows the segments of the result matrix created by all the *threadgroups* in the different steps in FP16 mode.

No new SASS instructions was introduced for *wmma.load* and *wmma.store* PTX instructions. In the SASS code, these instructions are broken down into a group of loads (LD.E.64, LD.E.128, LD.E.SYS) and normal stores(ST.E.SYS). The *wmma.load.c* PTX instruction is always broken into a group of normal loads(LD.E.SYS) whereas for operand matrices A and B it can be broken into a group of either four 64bit loads(LD.E.64) or two 128bit loads (LD.E.128) which depend on the layout in which the operand matrix is stored.

III. TURING TENSOR CORES

NVIDIA released the next generation of Tensor Cores in Turing GPU. They have maintained the backward compatibility to the Volta binaries, but there are significant architectural changes incorporated in Turing Tensor Cores. They have added support for two new precision modes, 4bit and 8bit, for machine learning inference workload. 8bit and 16bit mode support two new tile size $32 \times 8 \times 16$ and $8 \times 32 \times 16$ in addition to the original $16 \times 16 \times 16$ tile whereas the only tile size supported in 4bit mode is $8 \times 8 \times 32$.

Matrix distribution over fragments has changed in the Turing Tensor Core. It has a simple distribution compared to the Volta Tensor Core. For the input tile size $32 \times 8 \times 16$ and $8 \times 32 \times 16$, matrix layout does not affect the tile distribution among the *threadgroups* in the 16 and 8bit mode. In both modes for all the tile configuration, each row or column (depending on the mode and the operand matrix) is loaded by a *threadgroup* and eight consecutive *threadgroups* load eight consecutive row or column as shown in Figure 7. For matrices A and B, each thread inside a *threadgroup* loads four elements, whereas for matrix C each thread loads four elements in 16bit mode and two elements in 8bit mode.

For the Turing architecture, NVIDIA has provided a similar SASS interface for all the different modes and the tile size. Irrespective of the modes and tile size(except for 4bit mode), each *wmma.mma* PTX instruction disassembled into a group of four HMMA instructions whereas in the 4bit mode it disassembled into a single HMMA instruction.

Each HMMA instruction corresponds to a particular set as discussed in the previous section. The concept of steps in HMMA instructions has been abstracted away from the SASS assembly, and it might be sequenced through the different steps with a small state machine internally inside the Tensor Cores. For decoding the sets in this new interface, we developed a custom kernel for all the different modes and the tile size as described in the previous section.

Figure 8 shows the computation done in the different set in the 8bit and 16bit modes for all the different tile size. The computation for the 4bit mode is not shown since there is only one set(single HMMA instruction) in 4bit mode and the entire matrix MACC operation is performed in a single set. The computation performed in the 16bit mode for all

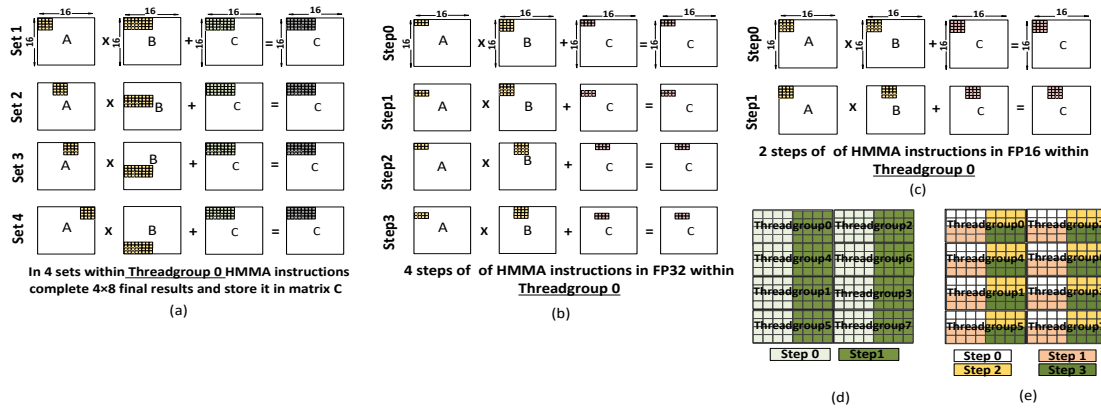


Fig. 6: The portion of matrix C calculated in the different sets and steps in V100 GPU

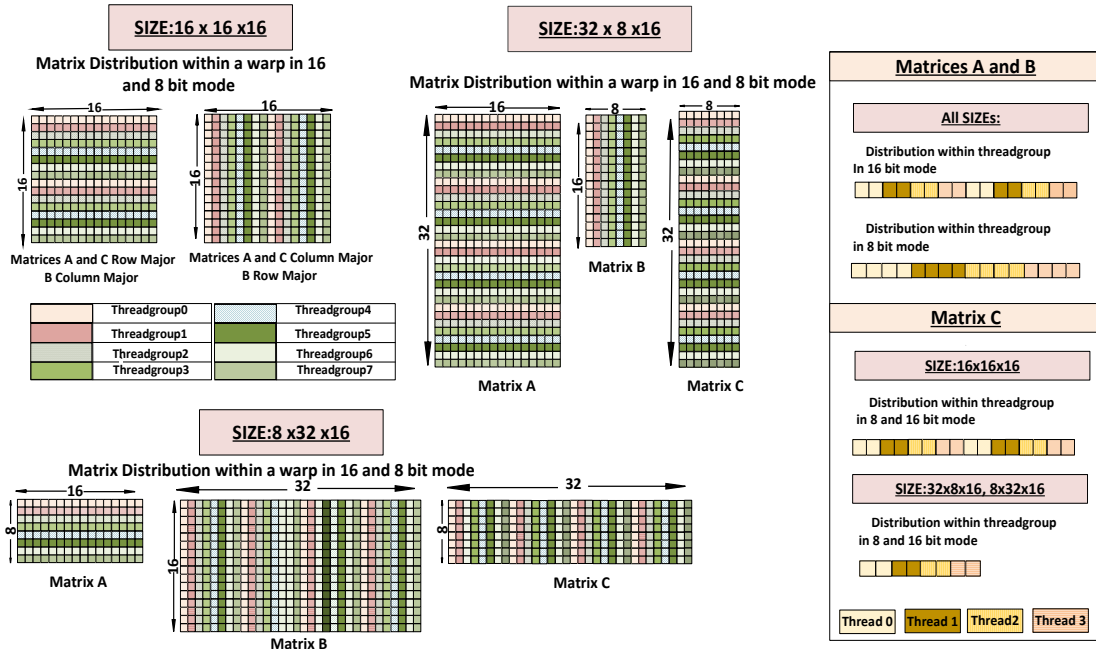


Fig. 7: Distribution of matrix fragment A,B and C for all the modes and tile configuration in RTX2018(Turing) GPU

the different tile size is the outer product between two input fragment. The computation performed in SET 1 is the outer product between the 16×8 fragment of matrix A with the 8×8 fragment of matrix B for the tile size $16 \times 16 \times 16$ as shown in 8a. In the 8bit mode, the computation performed in the different set is the product between the 8×16 fragment of matrix A with 16×8 fragment of matrix B. Internally Tensor Core may be performing the matrix multiplication using the outer product formulation. We have also calculated the average the average cumulative clock cycles for the different set for all the different modes and configuration as shown in Table I. The interesting observation is that the clock cycles needed for performing matrix MACC operation for tile size $16 \times 16 \times 16$ is more than that of V100 Tensor Cores. In the Turing Tensor Core the performance of mixed precision FP16 mode is less than the pure FP16 mode, and the 8bit mode is the fastest mode for performing the matrix MACC operation. The most

striking observation is that the 4bit mode is the slowest of all the mode. It may be because that since this mode is released as an experimental feature in Turing GPU and fully optimized implementation may be released in the future generation GPUs.

IV. DISCUSSION

In the previous section, we discussed the Tensor Cores in Volta and Turing GPU and explained the difference between the sets and steps and their role in matrix MACC operation for all the modes of operation and different tile configuration for this two architecture. From this section onwards we are only considering the Volta Tensor Cores since execution details of Volta Tensor Cores is transparent compared to Turing GPUs. In this section, we will explain why Nvidia has broken the execution of sets and steps in this way in Volta Tensor Cores.

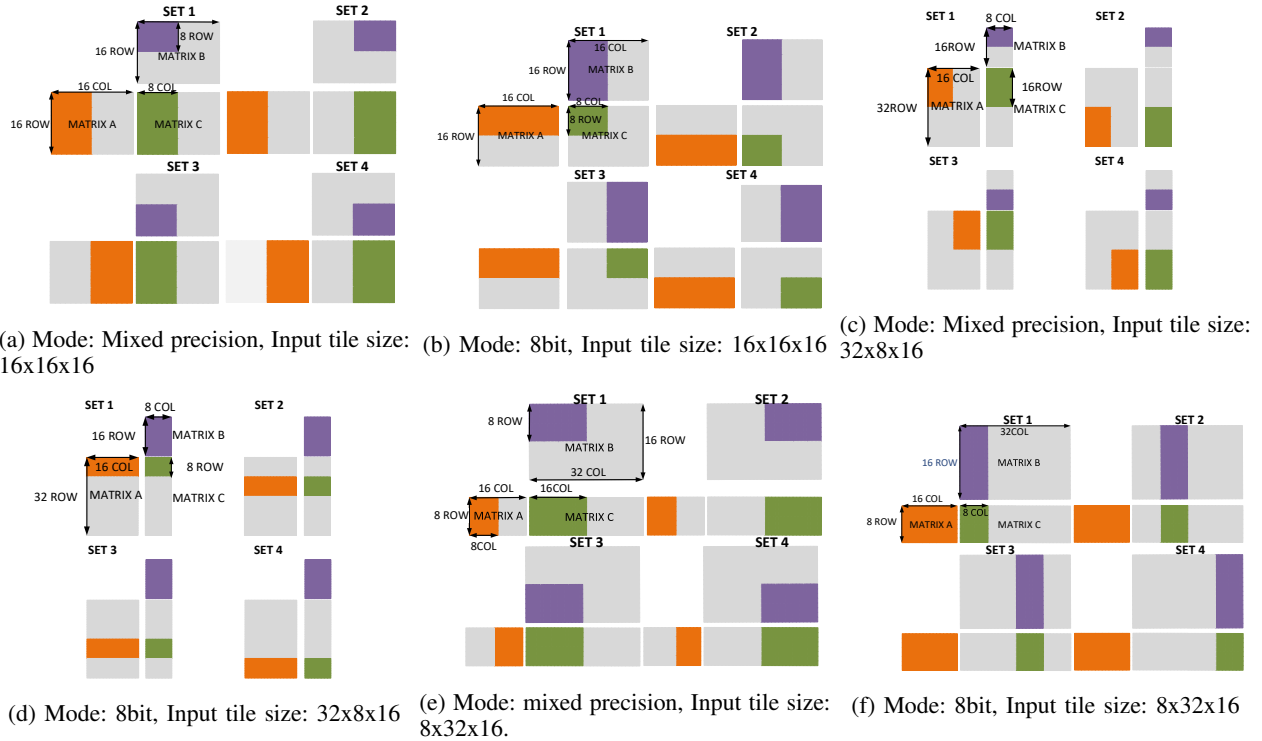


Fig. 8: The computation performed during the different sets(for all the different configuration) in RTX2080(Turing GPU)

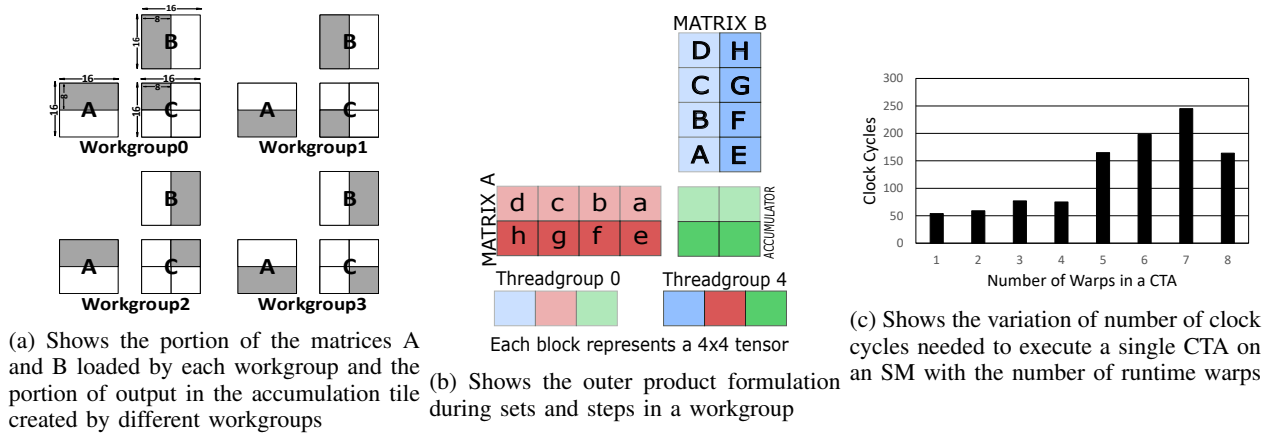


Fig. 9

At the end of this section, we propose a design for Tensor Core satisfying all the design requirement that we find in it.

To find the reason behind why NVIDIA is wasting the register bandwidth, we wrote a kernel to discover how the fragments of the different threads in a warp are used during the 16×16 matrix MACC operation. For example, for finding when the elements of the thread 0 fragment are used we altered the value of the operand matrix A fragment in thread 0 after `load_matrix_sync` and see how the result matrix is getting affected. Similarly, we wrote a kernel for all the other threads.

Our experiment demonstrates that *threadgroups* work in a pair to create 8×8 portion of the result matrix. We call the

pair of *threadgroups* working together *workgroup*. It is different from the OpenCL workgroup. The difference between the *threadgroup* and *workgroup* is that the *threadgroup* is only responsible for loading a portion of the operand matrix to its register (as shown in Figure 4) but they can't work independently to create the result matrix whereas every *workgroup* works independently to create a distinct portion of the result matrix. Only the threads inside the *workgroup* share the data, and thus different *workgroup* can work independently. There is a total of 4 *workgroups* in a warp and each *workgroup* is responsible for 8×8 segment of the result matrix.

Table II shows the pair of *threadgroup* constituting each

TILE SIZE (MxNxK)	PRECISION	Average Cumulative Clock Cycles			
		SET 1	SET 2	SET 3	SET 4
16x16x16	16Bit(FP32 Acc)	42	56	78	99
	16Bit(FP16 Acc)	44	52	60	74
	8Bit	40	44	47	59
32x8x16	16Bit(FP32 Acc)	48	60	81	104
	16Bit(FP16 Acc)	44	52	60	74
	8Bit	52	55	59	73
8x32x16	16Bit(FP32 Acc)	42	56	77	99
	16Bit(FP16 Acc)	42	50	58	72
	8Bit	38	42	46	56
8x8x32	4Bit	230	-	-	-

TABLE I: Shows the average cumulative clock cycles needed to execute the nth HMMA in the disassembled SASS instructions. Acc is abbreviation for accumulation i.e. Matrix C is stored in FP32 format

Work-group	Threadgroup	Matrix A	Matrix B
0	0 and 4	[0:7,0:15]	[0:15,0:7]
1	1 and 5	[8:15,0:15]	[0:15,0:7]
2	2 and 6	[0:7,0:15]	[0:15,8:15]
3	3 and 7	[8:15,0:15]	[0:15,8:15]

TABLE II: Shows the pair of threadgroup working together in different workgroup

workgroup, which in general can be formulated as $workgroupX = threadgroupX \cup threadgroupX+4$ where X is between 0 and 3. Table II also uses the notation [Row_Start : Row_End, Col_Start : Col_End] to show the portion of the operand matrices A and B loaded by the threads inside each *workgroup*. The elements loaded by the *workgroup* remains the same irrespective of the layout in which the operand matrix A, B and C are stored. Each *workgroup* has eight consecutive entire row of matrix A i.e. 8×16 tensor, eight consecutive full column of matrix B i.e. 16×8 tensor and 8×8 portion of the accumulator tile as shown in Figure 9a.

As demonstrated in table II each element of the matrices A and B are loaded twice by the threads in a warp. To clearly illustrate how *workgroups* work independently and why NVIDIA has broken the execution of sets and steps in this way, we go through more details about how *workgroup* use matrix elements in different sets and steps.

In each set, every *workgroup* performs the outer product between input tensors as shown in Figure 9b. For example in set 1 the outer product between input tensors $[a, e]$ and $[A, E]$ is completed to generate the partial result $[aA], [aE], [eA]$ and $[eE]$. Note that to create the partial product $[aE]$ *threadgroup* 0 needs the matrix B tensor (tensor E) which is only loaded by the *threadgroup* 4 and similarly to create $[eA]$, *threadgroup* 4 needs the matrix B tensor (tensor A) which is only loaded by the *threadgroup* 0, so as we see *threadgroups* can't work independently while *workgroups* can. Table table:2 is a general table for 9b, it shows the outer products which is done by a *threadgroup* during each sets and steps.

SET	STEP	Threadgroup X	Threadgroup X+4
1	0	$a[0:1] \times A$	$e[0:1] \times A$
	1	$a[2:3] \times A$	$e[2:3] \times A$
	2	$a[0:1] \times E$	$e[0:1] \times E$
	3	$a[2:3] \times E$	$e[2:3] \times E$
2	0	$b[0:1] \times B$	$f[0:1] \times B$
	1	$b[2:3] \times B$	$f[2:3] \times B$
	2	$b[0:1] \times F$	$f[0:1] \times F$
	3	$b[2:3] \times F$	$f[2:3] \times F$
3	0	$c[0:1] \times C$	$g[0:1] \times C$
	1	$c[2:3] \times C$	$g[2:3] \times C$
	2	$c[0:1] \times G$	$g[0:1] \times G$
	3	$c[2:3] \times G$	$g[2:3] \times G$
4	0	$d[0:1] \times D$	$h[0:1] \times D$
	1	$d[2:3] \times D$	$h[2:3] \times D$
	2	$d[0:1] \times H$	$h[0:1] \times H$
	3	$d[2:3] \times H$	$h[2:3] \times H$

TABLE III: Shows the pair of threadgroup working together in different workgroup

A. Tensor Core Design

According to the VOLTA white paper Tensor Core is performing 4×4 matrix MACC per cycle which can be translated into performing sixteen four elements dot products per cycle. We showed in Figure 5 that HMMA instruction for each step takes 2 cycles (steady state) and in each step every *threadgroup* generates 2×4 output matrix (Figure 6). So in each step *threadgroup* is performing 8, four-elements dot products per 2 cycle. Thus in a warp HMMA instruction is generating 32 dot products per cycle. Since Tensor Cores can only perform 16 four-elements dot products per cycle, so each warp must be allocated to 2 Tensor Cores. We have confirmed this experimentally. Figure 9c clearly indicates that only four warp can concurrently execute on a single SM, but V100 SM has 8 Tensor Cores per SM. Therefore each warp must be allocated to 2 Tensor Cores.

In order to propose a design for the Tensor Core, we need to calculate the register fetch bandwidth of it. Steady state latency of HMMA instruction is 2 clock cycles and there are three source operands and as we discussed earlier every thread fetches a pair of registers for each source operand. Therefore, the total fetch bandwidth provided by HMMA instruction is 6kB per 2 clock cycle per warp. This bandwidth is sufficient to fetch eight 2×4 FP16 tensor for operand A, eight 4×4 FP16 tensor for operand B and eight 2×4 FP32 tensor for operand C or eight 4×4 FP16 tensor for operand C (Figure 6) per warp per 2 clock cycles. But since every warp is allocated to 2 Tensor Cores, thus the register bandwidth needed per Tensor Core is 1.5kB per clock cycle per warp.

In Volta INT and FP32 instruction can be co-issued therefore there must be separate SIMD lanes for these cores whereas Tensor Core instruction cannot be co-issued with the integer and floating point arithmetic instructions thus Tensor Core may be using the associated buses with the INT and FP32 core. In our proposed design we are assuming that the Tensor Core shares the INT and FP32 SIMD lanes. There are 64 INT and 64 FP32 core inside V100 SM, thus a total of

128 SIMD lanes for every operand lane. As there are eight Tensor Core inside an SM thus only 16 32bit-lanes/Tensor Core for each source operand. Since there are 3 operand lane therefore the total fetch register fetch bandwidth of Tensor Core is 1.5kB/cycle satisfying the above requirement.

Figure 10 shows our proposed Tensor Core design. As discussed before each warp is allocated to 2 Tensor Cores so only two *workgroups* is allocated to each Tensor Core. Since 16 SIMD lanes are dedicated to each Tensor Core, eight lanes are dedicated to each workgroup, and four to each *threadgroup*. Each *threadgroup* lane fetches the operands to its buffer as shown in Figure 10. For operands 1 and 3, each *threadgroup* fetches the operands to its separate buffer whereas for operand 2 both the *threadgroups* fetches to a shared buffer. Mode of operation and steps will decide the *threadgroup* lane from which operand will be fetched. These buffers feed the 16 FP16 four-term dot product unit inside Tensor Core. In the dot product unit, the multiplication is being done in parallel, but the accumulation part is arranged over three stages resulting in a total of four stages. Since Tensor Core consists of 16 of FP16 four-term dot product units, it is capable of performing 4×4 matrix multiplication each cycle.

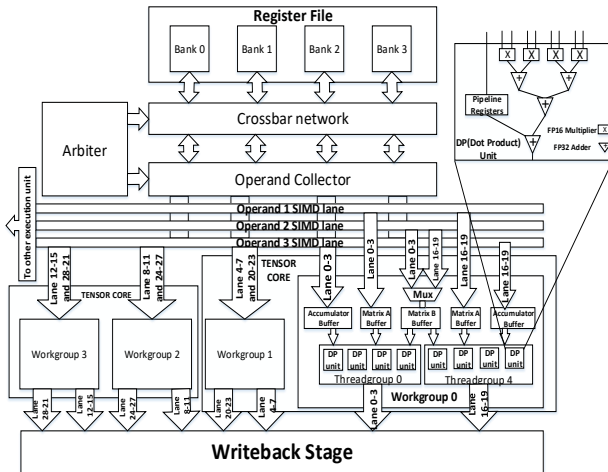


Fig. 10: Proposed Tensorcore Architecture

V. PROFILING TENSOR CORES

In the previous sections, we reviewed and discussed the different PTX and SASS instructions introduced in CUDA 9.0 to support the Tensor Cores and proposes an architectural model to fit in the current GPU pipeline. In this section, we will present and discuss the experimental results and the performance gains obtained by Tensor Cores over the standard Cuda Cores.

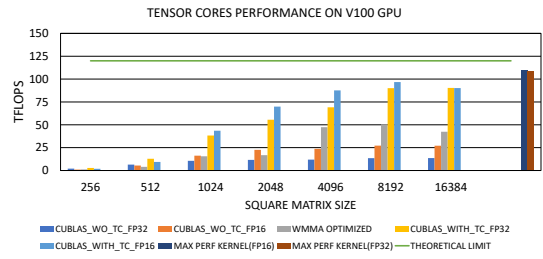


Fig. 11: Tensor Cores Performance

Although NVIDIA claims that the Tensor Cores provides the theoretical performance of 125 TFLOPs, the maximum performance for a GEMM kernel obtained in our experiments is around 96 TFLOPs. Maximal performance was observed for a square matrix of size 8192×8192 in FP16 mode. For measuring the maximum practical performance of Tensor Cores for any kernel, we developed a highly compute-intensive kernel with the computational intensity in order of 10^8 and launched a sufficient number of blocks and warps to keep the SMs busy and hide the long memory latency. The performance obtained for this `max_perf_kernel` was 109.6 TFLOPs for the FP16 mode and 108.7 TFLOPs for the FP32 mode.

Figure 11 shows the performance achieved by the Tensor Cores in different cases: a WMMA GEMM implementation and a cuBLAS library GEMM kernel with and without Tensor Cores. WMMA GEMM include optimizations like using shared memory and proper memory layout. The performance gain obtained using the cuBLAS GEMM kernel is more than WMMA GEMM implementation (both the kernels using Tensor Cores) since cuBLAS is a highly optimized library which had the optimization to avoid the shared memory bank conflict and employ software pipelining. Tensor Cores provide a performance boost of about $3 - 6 \times$ times that of SGEMM (Single Precision GEMM) kernel and about $3 \times$ that of HGEMM (Half Precision GEMM) kernel both on Cuda Cores.

We also profile the latency of each instruction for different matrix sizes, Figure 12 demonstrates one of our profiling results. The Figure shows the latency of `wmma.load`, `wmma.store` and `wmma.mma` instructions during several iterations of WMMA kernel (kernel uses shared memory and perform matrix MACC operation on the square matrix of size 1024). All the three graphs show some outlier warp being starved due to the scheduling policies and high memory traffic. Another important observation is that the minimum latency of `wmma.load`, `wmma.store` and `wmma.mma` instruction is 125, 120 and 70 clock cycles respectively due to the different behavior of these instructions. In Figure 13 we choose the median to illustrate how the latency of `wmma.store`, `wmma.mma`, `wmma.load` instruction varies with the matrix size for WMMA kernels. In Figure 13 `wmma:load` latency is drawn on a logarithmic axis whereas the rest of the graph is drawn on the normal axis.

Figure 13 shows that shared memory reduces the median `wmma:load` latency by a factor of more than 100 for WMMA

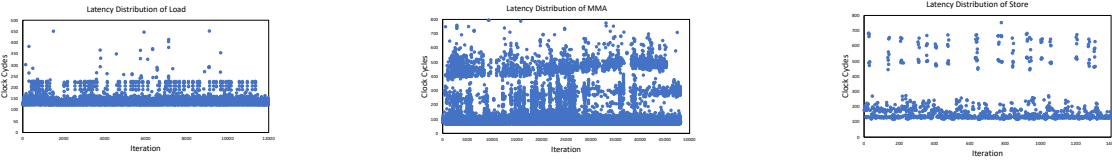


Fig. 12: Latency distribution of *wmma:load*, *wmma:mma* and *wmma:store* instructions for gemm kernel (square matrix size 1024) using shared memory

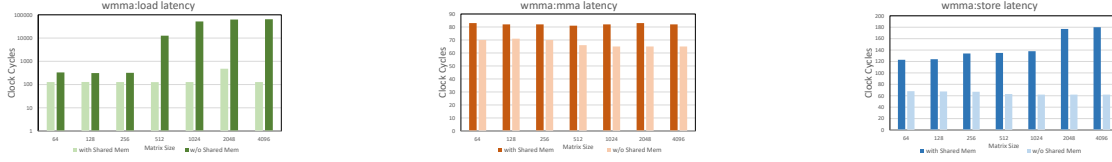
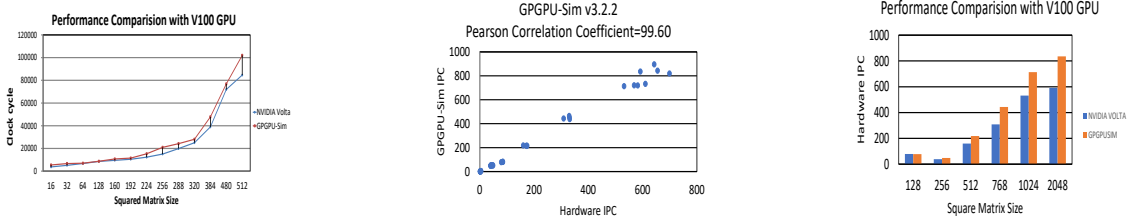


Fig. 13: Shows the variation of latency of *wmma:load*, *wmma:mma* and *wmma:store* instructions with matrix size



(a) Variation of clock cycles of a gemm kernel on GPGPU-Sim with the different input size (b) Coorelation of gemm kernels created using the cutlass template on GPGPU-Sim created vs real V100 GPUs (c) Variation of IPC of gemm kernels using the cutlass template on GPGPU-Sim vs real V100 GPU

Fig. 14

kernel operating on a larger matrix. The slow global memory access is replaced by fast shared memory access, thus for larger kernel when the memory traffic is high the overall throughput for processing memory request is drastically increased with shared memory.

VI. MODELLING TENSOR CORES

We modeled the Volta Tensor Cores on GPGPU-Sim (Version 3.2) [23]. We extended the current version of GPGPU-Sim to support the half-precision datatype by using the half-precision C++ header-only library hosted on SourceForge.net [24]. The library provides an efficient implementation of an FP16 type conforming to the IEEE 754 half-precision format as well as provide common arithmetic operators and type conversion. We implemented all the three PTX instructions: *wmma.load*, *wmma.store* and *wmma.mma* introduced for Tensor Cores. The *wmma.load* and *wmma.store* conform the matrix distribution shown in Figure 4. We also validated our modeled Tensor Core against Nvidia Tesla V100’s Tensor Core connected to Intel(R) Core(TM) i7-4771 CPU @ 3.50GHz host. The host is running Ubuntu 16.04.4 LTS and has CUDA Driver Version 9.0 with CUDA Capability 7.0. The GNU compiler version for compiling the host code is 4.9.4.

Figure 14a shows how the clock cycles required by matrix multiply and accumulate kernel using the WMMA API varies with the matrix size on the actual V100 GPU and GPGPU-Sim. From the graph its evident that GPGPU-Sim is modeling

the kernel quite accurately with a standard deviation of less than 5

VII. CUTLASS

Deep learning is a rapidly developing field, and a plethora of deep learning algorithms are present in the literature and thus experimenting with different cases and finding the best possible algorithm and efficiently implementing on GPU is extremely common. In order to increase the productivity of developer, NVIDIA introduced the CUTLASS library. It is an open-source CUDA C++ template library for efficient linear algebra in C++. This library provides the basic building block for implementing high-performance fused matrix multiply kernel for deep learning workloads.

We have enabled CUTLASS library on GPGPUSIM for micro-architectural investigation of machine learning workloads. Nvidia has provided unit test-suite for CUTLASS library consisting of around 680 test case. We have been able to run these test cases on GPGPUSIM. We have also calculated the correlation of the IPC (Instructions per Clock) on GPGPUSIM versus that of real NVIDIA V100 GPUs for WMMA kernel developed using the template provided in the CUTLASS library. GPGPUSIM 3.2 obtained an IPC correlation of 99.60% as shown in the Figure 14b and Figure 14c.

VIII. CONCLUSION

The rising market for deep learning application has pushed NVIDIA to boost the performance of the dense matrix computation on GPU. Recently, NVIDIA released the Volta micro-architecture featuring specialized computing units called Tensor Core. This paper presented the detailed micro-architectural characterization and analysis of the Tensor Core and proposes an architectural model on top of an existing GPU pipeline. We have done extensive profiling to find out the architectural details of the Tensor Core and modeled our proposed architectural model for Volta Tensor Cores on GPGPU-Sim with 99.6% correlation of IPC with the real V100 GPU. We also enabled the NVIDIA Cutlass library, open-source CUDA C++ template library supporting Tensor Cores, on GPGPU-Sim. We believe that our proposed architecture models the Tensor Core quite accurately and will serve as a promising direction for further micro-architectural investigation of machine learning workloads.

REFERENCES

- [1] A. Graves, A.-r. Mohamed, and G. Hinton, "Speech recognition with deep recurrent neural networks," in *Acoustics, speech and signal processing (icassp), 2013 IEEE international conference on*, pp. 6645–6649, IEEE, 2013.
- [2] A. Bordes, X. Glorot, J. Weston, and Y. Bengio, "Joint learning of words and meaning representations for open-text semantic parsing," in *Artificial Intelligence and Statistics*, pp. 127–135, 2012.
- [3] S. Ren, K. He, R. Girshick, and J. Sun, "Faster r-cnn: Towards real-time object detection with region proposal networks," in *Advances in neural information processing systems*, pp. 91–99, 2015.
- [4] K. Simonyan and A. Zisserman, "Very deep convolutional networks for large-scale image recognition," *arXiv preprint arXiv:1409.1556*, 2014.
- [5] O. Vinyals, A. Toshev, S. Bengio, and D. Erhan, "Show and tell: A neural image caption generator," in *Proceedings of the IEEE conference on computer vision and pattern recognition*, pp. 3156–3164, 2015.
- [6] K. Kavukcuoglu, P. Sermanet, Y.-L. Boureau, K. Gregor, M. Mathieu, and Y. L. Cun, "Learning convolutional feature hierarchies for visual recognition," in *Advances in neural information processing systems*, pp. 1090–1098, 2010.
- [7] N. P. Jouppi, C. Young, N. Patil, D. Patterson, G. Agrawal, R. Bajwa, S. Bates, S. Bhatia, N. Boden, A. Borchers, *et al.*, "In-datacenter performance analysis of a tensor processing unit," in *Computer Architecture (ISCA), 2017 ACM/IEEE 44th Annual International Symposium on*, pp. 1–12, IEEE, 2017.
- [8] T. Chen, Z. Du, N. Sun, J. Wang, C. Wu, Y. Chen, and O. Temam, "Diannao: A small-footprint high-throughput accelerator for ubiquitous machine-learning," *ACM Sigplan Notices*, vol. 49, no. 4, pp. 269–284, 2014.
- [9] Y.-H. Chen, J. Emer, and V. Sze, "Eyeriss: A spatial architecture for energy-efficient dataflow for convolutional neural networks," in *ACM SIGARCH Computer Architecture News*, vol. 44, pp. 367–379, IEEE Press, 2016.
- [10] S. Chakradhar, M. Sankaradas, V. Jakkula, and S. Cadambi, "A dynamically configurable coprocessor for convolutional neural networks," *ACM SIGARCH Computer Architecture News*, vol. 38, no. 3, pp. 247–257, 2010.
- [11] M. M. Khan, D. R. Lester, L. A. Plana, A. Rast, X. Jin, E. Painkras, and S. B. Furber, "Spinnaker: mapping neural networks onto a massively-parallel chip multiprocessor," in *Neural Networks, 2008. IJCNN 2008.(IEEE World Congress on Computational Intelligence). IEEE International Joint Conference on*, pp. 2849–2856, Ieee, 2008.
- [12] C. Farabet, C. Poulet, J. Y. Han, and Y. LeCun, "Cnp: An fpga-based processor for convolutional networks," in *Field Programmable Logic and Applications, 2009. FPL 2009. International Conference on*, pp. 32–37, IEEE, 2009.
- [13] D. Kim, J. Kung, S. Chai, S. Yalamanchili, and S. Mukhopadhyay, "Neurocube: A programmable digital neuromorphic architecture with high-density 3d memory," in *Computer Architecture (ISCA), 2016 ACM/IEEE 43rd Annual International Symposium on*, pp. 380–392, IEEE, 2016.
- [14] C. Zhang, P. Li, G. Sun, Y. Guan, B. Xiao, and J. Cong, "Optimizing fpga-based accelerator design for deep convolutional neural networks," in *Proceedings of the 2015 ACM/SIGDA International Symposium on Field-Programmable Gate Arrays*, pp. 161–170, ACM, 2015.
- [15] nvidia, "volta-whitepaper," 2017.
- [16] nvidia, "Volta: Programmability and performance," 2017.
- [17] nvidia, "cublas developer guide," 2008.
- [18] nvidia, "cudnn developer guide," 2014.
- [19] S. Chetlur, C. Woolley, P. Vandermersch, J. Cohen, J. Tran, B. Catanzaro, and E. Shelhamer, "cudnn: Efficient primitives for deep learning," *arXiv preprint arXiv:1410.0759*, 2014.
- [20] nvidia, "Cutlass: Fast linear algebra in cuda c++," 2017.
- [21] nvidia, "cutlass," 2018.
- [22] Z. Jia, M. Maggioni, B. Staiger, and D. P. Scarpazza, "Dissecting the nvidia volta gpu architecture via microbenchmarking," *arXiv preprint arXiv:1804.06826*, 2018.
- [23] A. Bakhoda, G. L. Yuan, W. W. Fung, H. Wong, and T. M. Aamodt, "Analyzing cuda workloads using a detailed gpu simulator," in *Performance Analysis of Systems and Software, 2009. ISPASS 2009. IEEE International Symposium on*, pp. 163–174, IEEE, 2009.
- [24] C. Rau, "Half-precision floating point library," 2017.